Annals of Nuclear Energy 192 (2023) 109973

Contents lists available at ScienceDirect

Annals of Nuclear Energy

journal homepage: www.elsevier.com/locate/anucene

Towards preliminary design calculations with TRANSURANUS for application of Hastelloy cladding material

A. de Lara [a], A. Schubert [b], E. Shwageraus [a], P. Van Uffelen [b,*]

[a] Department of Engineering, University of Cambridge, Cambridge, United Kingdom
[b] European Commission, Joint Research Centre (JRC), Karlsruhe, Germany

ARTICLE INFO

Keywords:
Advanced technology fuel
MSR
FLiBe
Hastelloy-N
Cladding

ABSTRACT

This study summarises the work performed to implementing the material properties for Hastelloy-N, of interest for GenIV MSRs, into the TRANSURANUS fuel performance code. The individual development of correlations on the basis of experimental data in the open literature, and the subsequent assessment with an independent dataset when available, also revealed the need for specific new experiments that have been pointed out. Following that, an integral assessment of the new code version was carried out as well. The simulation of a biaxial cladding burst tests from ORNL, with due consideration of the uncertainties and analysis by means of the new graphical output analysis tool TUPython for uncertainty and sensitivity analysis, provided encouraging results for the preliminary implementation of Hastelloy-N properties. The proposed set of material properties can therefore be readily implemented in any other fuel performance code.

1. Introduction

Generation IV (GenIV) was a concept developed at the early 2000s by the countries conforming the Generation IV International Forum (GIF) involving a series of reactor concepts that take into account at least one of the following considerations: sustainability to meet the carbon free objectives, increased efficiency; economic viability to compete with existing systems; safety and reliability; proliferation resistance and physical protection to reduce the risks of creating weapon usable materials. Among the proposed systems, the Molten Salt Reactor (MSR) its acknowledged to being the most inherently safe and flexible.

However, as most GenIV reactors, MSR concepts are not new since they were first developed in the 1950s at the Oak Ridge National Laboratory (ORNL) with the first (and only) test reactor operated in the 1960s. This reactor concept uses molten salt as fuel and/or coolant. If the latter case is applied, MSRs are re-branded as Fluoride Salt Cooled High Temperature Reactors (FHRs) which propose a coated fuelled core developed for High Temperature Gas cooled Reactors (HTGRs) cooled using fluoride molten salts. The FHR concept is a subclass of MSRs. While the latter has the fuel dissolved in the fluoride salt coolant, the FHR uses solid fuel physically separated from the molten coolant salt. Amongst different proposals for the FHR fuel design, a traditional solid pin-type fuel configuration has been explored (Greene et al., 2010; Xing, 2022). However, the use of metallic cladding would come with corrosion-related issues.

According to the latest GIF report, Kamide et al. (2021), one of the R&D objectives of MSRs (and FHRs) is the research of materials compatible with molten salt. Using salt as coolant results in a higher average temperature with lower temperature gradient across the core. On the other hand, the use of molten salt results in extreme environments due to the high temperature and high corrosion involved which affects the performance of the fuel and materials. Such harsh conditions require the consideration of advanced accident tolerant cladding materials in a similar way as for LWRs analysed in the frame of the R2CA project. This project aims at the reduction of the radiological consequences of accidents. To this end, the R2CA project aims at the evaluation of promising enhanced-accident fuels and materials, including coated claddings as well as Fe based or Ni based alloys.

The development of materials that can withstand both high temperature and high corrosive environments is essential for MSRs. Such materials should exhibit minimum corrosion when exposed to the molten salt as well as creep strength at operating temperatures (Guo et al., 2018) and applied inner cavity loads. Given the extreme temperatures, the use of a passivating oxide layer (Guo et al., 2018) is restricted. Therefore, the use of stainless steel in MSRs is subjected to corrosion related issues. Some experiments were conducted in the 1960's by the Aircraft Nuclear Propulsion Program (ANPP) (Haubenreich and Engel, 1970) and Molten Salt Reactor Experiment (MSRE) (Smith, 1965) showing that Nickel has the best corrosion resistance when exposed to FliBe,

* Corresponding author.
E-mail addresses: ad2048@cam.ac.uk (A. de Lara), Arndt.SCHUBERT@ec.europa.eu (A. Schubert), es607@cam.ac.uk (E. Shwageraus), Paul.VAN-UFFELEN@ec.europa.eu (P. Van Uffelen).

https://doi.org/10.1016/j.anucene.2023.109973
Received 12 January 2023; Received in revised form 17 April 2023; Accepted 5 June 2023
Available online 22 June 2023

Table 1
Nominal Composition of HASTELLOY-N alloy (UNS N10003) in wt% (Swindeman et al., 2014a).

Element	Ni	Cr	Mo	Fe	Si	Mn	V	C	Co	Cu	W	Al+Ti
wt%	71 Bal	7	16	4 (max)	1 (max)	0.8 (max)	0.5 (max)	0.06	0.02 (max)	0.35 (max)	0.5 (max)	0.5 (max)

an eutectic mixture of 2LiF-BeF2 (Scarlat et al., 2014). However its mechanical performance shown to be poor when exposed to operating temperatures above 650 °C. The solution was the development of a series of Ni-Mo-Cr alloys where Mo provides high temperature strength so as Cr together with oxidation resistance (Smith, 1965).

In particular, INOR-8 currently known as Hastelloy-N or Alloy-N (Swindeman et al., 2014a) (UNS N10003) developed by Oak Ridge National Laboratory (ORNL) in the 1950s[1] has demonstrated good oxidation resistance to hot fluoride salts (in the temperature range of 704 to 871 °C) (Swindeman et al., 2014a). In addition, since materials are going to be exposed to radiation due to the fission reactions taking place in the reactor, the alloy needs to be resistant to irradiation to prevent from swelling and irradiation induced (or enhanced) creep.

The composition of the material is displayed in Table 1. The alloy is solution strengthened with a relatively high amount of Mo. Si contributes to stabilising the Ni_2Mo_4(C, Si) and Ni_3Mo_3(C, Si), primary precipitates in the alloy (Xu et al., 2015).

In this work, the material Hastelloy-N was added to the TRANSURANUS (TU) (Lassmann, 1992) fuel performance code, which we shortly introduce in the next section. In the subsequent section, we outline how the necessary correlations, using existing data available in literature, were created and tested at different temperatures, loads and in some cases under different levels of irradiation. This contributes to the data acquisition of enhanced accident tolerant materials and their evaluation as carried out in the R2CA project. Once implemented, the behaviour of the material was compared to that of the same material using different sources or to other materials already existent in TU as means to verify its performance. This constitutes the first step in the validation process, where only the separate models are validated. However, given the lack of accessible up-to-date data, some correlations are subjected to high uncertainties as it will be developed in the following sections. For this reason, we took advantage of the in-built TU Monte Carlo capability to consider uncertainties when carrying out the first integral assessment of the code in the next section. For this purpose, a cladding burst test was performed and results were compared to a similar experiment carried out at ORNL (Stearns, 1967), taking into consideration all possible uncertainties. Finally, in the last section we draw the conclusions of this work and formulate recommendations for further research.

2. Fuel performance modelling technique

There are two main types of codes that model fuel performance: two dimensional and three dimensional (Van Uffelen et al., 2018). The former can be subdivided into three different categories. The first category is sometimes referred as "1.5D" code, these codes exploits the rotational symmetry of the fuel rod and include codes such as TU and ENIGMA (Jackson et al., 1990). The other category exploit finite element (or finite volumes) models making assumptions about either the azimuthal or the axial direction (Haynes, 2018). 3-D fuel performance codes such as BISON, a finite element based code capable of solving the fully-coupled equations of thermo-mechanics and species diffusion (Hales et al., 2016), can be used for one, two or three dimensions.

[1] It is important to clarify that Hastelloy-N is the commercial name of the alloy by ORNL. Czech MoNiCr, Chinese GH3535 and Russian HN80MTY are UNS N10003 as well.

The TU code for fuel performance can analyse a range of conditions of various fuel rod types. Its ease to handle and fast running times (Magni et al., 2021) makes it an ideal candidate for optimisation studies when a high number of possibilities want to be attempted. It can perform calculations in two different modes: deterministic or statistical, while guaranteeing numerical stability. It performs a thermal and mechanical analysis along the radial dimension of the fuel later coupled between a number of axial slices. TU relies on a series of in-built libraries and subroutines suitable for oxide, MOX, carbide and nitride fuels, different zirconium alloys and stainless steel claddings and different coolants including light water, sodium, potassium, lead, lead-bismuth and helium (Magni et al., 2021). However, materials used in MSRs are not yet developed. By introducing Hastelloy-N, the possibility of utilising TU for the development of new Gen-IV MSRs is envisaged.

3. Material properties

In order to implement Hastelloy-N to the TRANSURANUS code (Dickon et al., 2017), correlations describing its behaviour need to be added. Based upon data available in literature, (semi-)empirical relations have been created. Due to the lack of data, some properties have been adopted from existent TU materials that resemble the behaviour of the alloy.

In TU, the behaviour of the material is described using different correlations. For each correlation, either a constant value or a relation is required. The latter is created using MATLAB curve fitting toolbox (Qing-Wan, 2010) which uses the least squares fitting method. If a relation is created, the uncertainty of the coefficients is included. A table including all coefficients and uncertainties is shown in the Appendix (Table A.4).

In addition, since the behaviour of the material under irradiation is going to be assessed, a conversion factor between the dose level (dpa) and neutron fluence is required as TU works with fluence (n/cm^{2}s) and most experiments involved ion doses in dpa. To convert fluence to dpa, the conversion factor is conv = 5×10^{-22}, hence, 1dpa = 2×10^{21} n/cm^2 s as it roughly corresponds to that developed in a previous TU project and it also matches the relation from Field et al. (2015).

Once the correlation is created, a different set of data is used to verify whether the empirical relations agree. This is in line with the methodology applied for TRANSURANUS (Magni et al., 2021) and with the general principles of code verification and validation recommended in by Oberkampf and Roy (2010), where submodels are validated prior to the integral assessment of a code.

3.1. Constant properties

Due to the limited amount of data, the material is assumed to be isotropic. Hastelloy-N alloy has a face-centred cubic (FCC) crystal structure (Liu et al., 2019) which supports the assumption. Poisson's ratio for the alloy was found in Cen et al. (2019) for a temperature of 650 °C. Poisson's ratio vs temperature data for more temperatures was not available in literature. Since the temperature is within the operating temperature range of MSRs, the value was set to be constant in TU as a first approximation. Likewise, for the specific heat, data for Hastelloy was found (Anon, 2021) to be $c_p \approx 420$ J/g K and is applied as constant value.

According to Ref. Swindeman et al. (2014a), the density of the material is $\rho = 8.86$ g/cm^3 and the melting range is between 1300-1400 °C . According to other sources (Yadav, 2016; Anon, 2021), such range is 1325-1370 °C or a fixed value of 1327 °C respectively. The

Table 2
Material properties of Hastelloy-N.

Poisson's ratio	Specific heat (J/g K)	ρ (g/cm^3)	Melting range (°C)	Heat of melting (°C)	Emissivity
0.30	420.00	8.86	1327.00	298.16	0.25

melting point was chosen to be 1327 °C as it is included in all the ranges and it is also a conservative assumption. The heat of melting for Hastelloy-N is not available in the open literature. A study (Padalko et al., 2003) suggested assuming the heat of melting of Nickel (at 0.1 MPa) for this alloy $L = 17.5$ kJ/mol. TU requires J/g. The conversion from mol to g is performed using the molar mass of Ni which is 58.69 g, $L \approx 298.16$ J/g. The emissivity of Hastelloy-N is roughly $e \approx 0.25$ (Gordon et al., 2012).

These properties are summarised in Table 2.

3.2. Correlations depending on environmental conditions

3.2.1. Material behaviour under stress

The dynamic elasticity module for different temperatures is obtained from Swindeman et al. (2014a). The empirical correlation involves a third order polynomial that agrees with other materials in TU which use polynomials as well with orders ranging between first and fourth.

$$E = a \times T^3 + b \times T^2 + c \times T + d \tag{1}$$

where T is the temperature in °C and coefficients a, b, c and d are shown in Table A.4.

The last data point is 1000 °C, so the correlation is valid until that point. TU displays a warning message if the temperature goes over 1000 °C as it is not clear whether the correlation is accurate after that point. From 1000 °C until the melting point, the correlation continues to work. After the melting point, the temperature is fixed to the melting temperature of the alloy and it follows the following equation with χ (from 0 to 1) defining the state (liquid or solid):

$$E' = (1 - \chi)E(T_{\text{melt}}) + \chi E \tag{2}$$

Such linear combination for solid and liquid properties applied is an approximation that is applied consistently in the code for many material properties. To determine the stress at which the material starts to deform plastically (permanently deformed), the yield strength is calculated for different temperatures. For the yield strength two different sources were used (Venard, 1965) (with 0.2% offset) and Martin and Weir (1965) to get a broader temperature profile. The empirical relation is built from the mean of both data sets.

$$\text{Ys} = a \times T^3 + b \times T^2 + c \times T + d \tag{3}$$

where T is the temperature in °C and coefficients a, b, c and d are shown in Table A.4.

As the last data point is for a temperature of 1000 °C, if the temperature goes beyond, the value considered for the correlation is fixed to $T = 1000$ °C.

To determine the stress at which the material fails, the ultimate tensile strength (UTS) is calculated using data obtained from (Swindeman et al., 2014b). Following the procedure for 9Cr-ODS steel, since the fourth order polynomial used to fit predicts an increase of UTS after about 900 °C, a linear extrapolation is performed from that temperature in order to better represent the data. The analytical expression is as follows:

$$\text{UTS} = \begin{cases} a_1 \times T'^4 + b_1 \times T'^3 + c_1 \times T'^2 + d_1 \times T' + e_1 & T \leq 900\ ^\circ\text{C} \\ a_2 + b_2 \times (T - 800) & T > 900\ ^\circ\text{C} \end{cases} \tag{4}$$

where $T' = \frac{T - 537.6}{259.7}$ being 537.6 and 259.7 the mean and standard deviation of the data respectively.

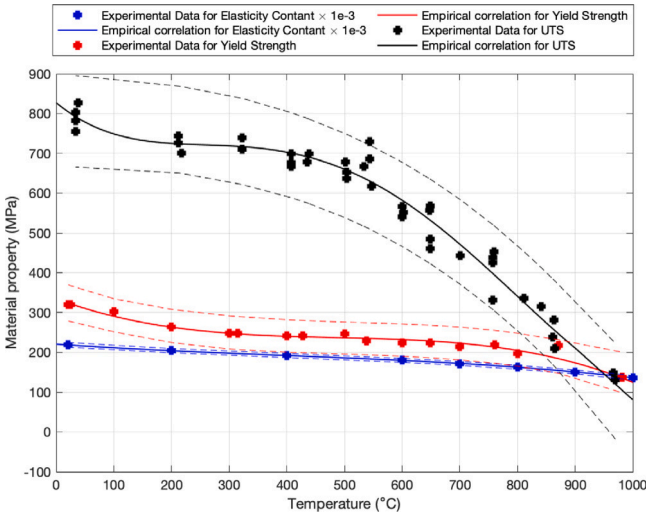

Fig. 1. In blue, dynamic modulus of elasticity (divided by 1000) from Swindeman et al. (2014a) and its empirical correlation (E/1000). In red yield strength from Venard (1965) and Martin and Weir (1965) and its empirical correlation (Ys). In black, UTS from Swindeman et al. (2014b) and its empirical correlation (UTS). The dashed lines show the confidence interval 95%.

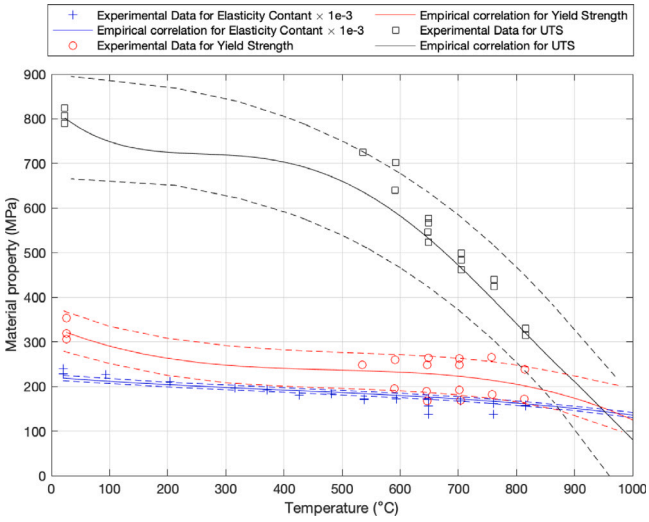

Fig. 2. In blue, dynamic modulus of elasticity (divided by 1000) and the empirical correlation developed (E/1000). In red yield strength and the empirical correlation developed (Ys). In black, UTS and the empirical correlation (UTS). All data is from Swindeman (1961). The dashed lines show the confidence interval 95%.

Results for the Elasticity Constant, Yield Strength and UTS are shown in Fig. 1. The confidence intervals (95%) of the fit are included.

To verify whether the empirical relations developed could replicate the behaviour of the alloy, a different set of data from experiments performed at ORNL (Swindeman, 1961) is used (Fig. 2).

The mean relative error between the empirical relations and the data from ORNL for the elasticity constant, the yield strength and the UTS is 6.3%, 15.0% and 5.5% respectively. The scattered yield strength and UTS data lies within the confidence intervals. The elasticity constant data is further away from the confidence interval since the data set

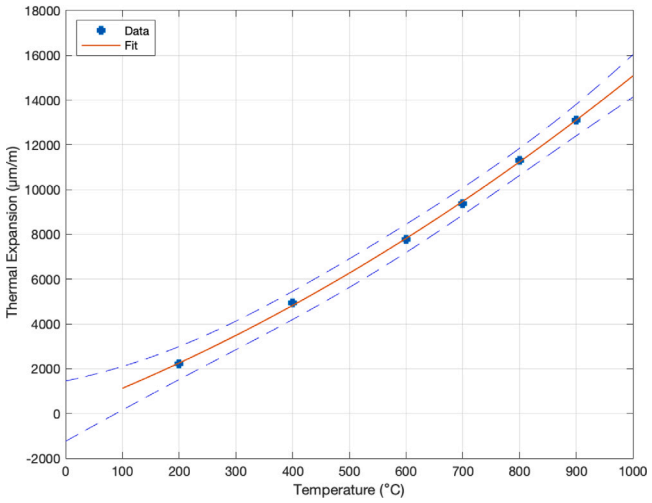

Fig. 3. Thermal expansion (um/m °C) for different temperatures in °CDdata from Swindeman et al. (2014a) is fitted. The dashed lines show the confidence interval 95%.

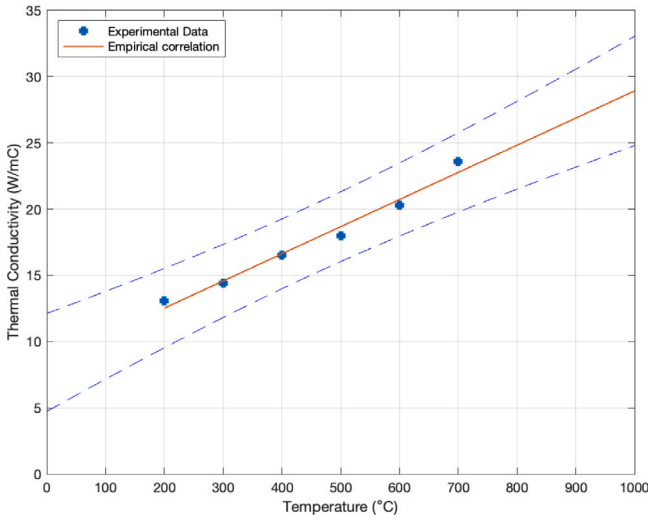

Fig. 4. Thermal Conductivity (W/m °C) for different temperatures in °CDdata from Swindeman et al. (2014a) is fitted. The dashed lines show the confidence interval of 95%.

from Swindeman et al. (2014a) converges in a third order polynomial while the data from Swindeman (1961) is more scattered. Taking into account that the data from Swindeman (1961) was obtained in the early 1960s, the agreement is satisfactory.

3.2.2. Temperature-related properties of the alloy

For the thermal strain, data is given in intervals (Swindeman et al., 2014a).

To calculate thermal expansion it is necessary to apply the following formula:

$$\epsilon = \alpha_{av}(T - T_0) \tag{5}$$

where α_{av} corresponds to the mean coefficient of thermal expansion (CTE) and T_0 is equal to 20 °C .

The empirical equation obtained by fitting the data from Swindeman et al. (2014a) is a second order polynomial which agrees with TU's correlations for different steels as shown in Fig. 3.

$$\epsilon = a \times T^2 + b \times T + c \tag{6}$$

Temperature is in degrees Celsius.

For the thermal conductivity, a first order polynomial is fitted (Fig. 4) following the procedure in TU for other metals. A linear correlation is supported if it is assumed that the phonon terms are negligible relative to the electronic component as it was done for the study of the thermophysical properties of U_3Si_2 (White et al., 2015). The assumption of linear electronic behaviour is expressed by the Wiedemann Franz law.

$$\kappa = a \times T + b \tag{7}$$

Using data from the 1960s (Watrous, 1961; Farkas, 1967), the developed empirical relations are tested in Fig. 5. For thermal expansion (blue), as the data used to create the empirical relation starts at 200 °C, the agreement is better for higher temperatures and it does not match as well for temperatures below that value, the mean absolute error decreases with increasing temperature, which is good considering the temperature range of application in FHRs.

For thermal conductivity, the correlation agrees for lower temperatures and diverts at temperatures higher than 300 °C. Data below 300 °C is within the confidence interval of the fit (dashed red line in Fig. 5). The average error is 12.4%. Although the correlation fails to agree, the experimental data shows an erratic behaviour as it does

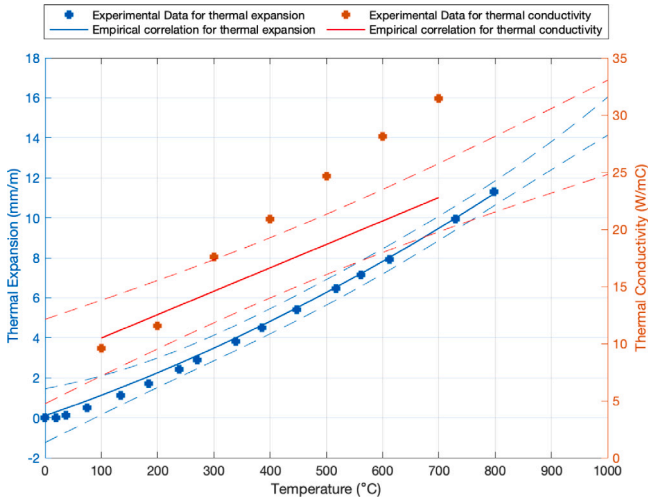

Fig. 5. Thermal expansion coefficient (mm/m °C) from Watrous (1961) and the developed correlation ϵ in blue. Thermal Conductivity (W/m °C) from Farkas (1967) and empirical correlation (κ) in red. The dashed lines show the confidence interval of 95%.

not exhibit a linear behaviour as it was expected from the literature (White et al., 2015). So the result is not conclusive and requires more experimental investigations.

3.2.3. Properties affected by irradiation

Swelling and creep are affected by radiation. Therefore, this dependence has to be appropriately captured.

Swelling Swelling is affected by temperature and irradiation. The correlation involves a temperature factor T_{factor} and a fluence factor $flux_{factor}$ converted from n/cm^2 to dpa using the conversion factor.

$$\Delta S = T_{factor} \times flux_{factor} \tag{8}$$

Starting from the fluence factor, data from Ref. Zhang et al. (2017) is used. Fig. 6 from the paper displays the volumetric swelling for the alloy.

The data obtained by the authors of Ref. Zhang et al. (2017) (red line in Fig. 6) is used and fitted as shown in Fig. 7.

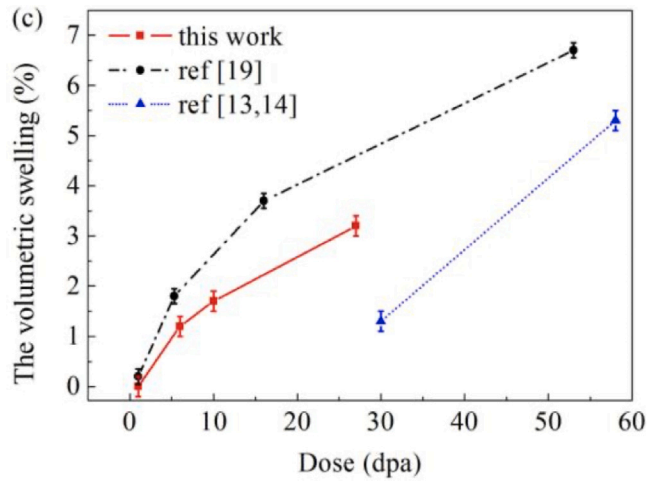

Fig. 6. Swelling rate from Zhang et al. (2017). Swelling percentage of irradiated samples as a function of dose (dpa): red squares from Zhang et al. (2017), the blue triangles from Ref. Guo et al. (2015) and Liu et al. (2015) ([13,14] in the legend of the Figure), the black circles show the swelling data about pure nickel from Ref. Jin et al. (2016) (Ref. [19] in the legend of the Figure). The experiments were performed at room temperature according to Zhang et al. (2017).

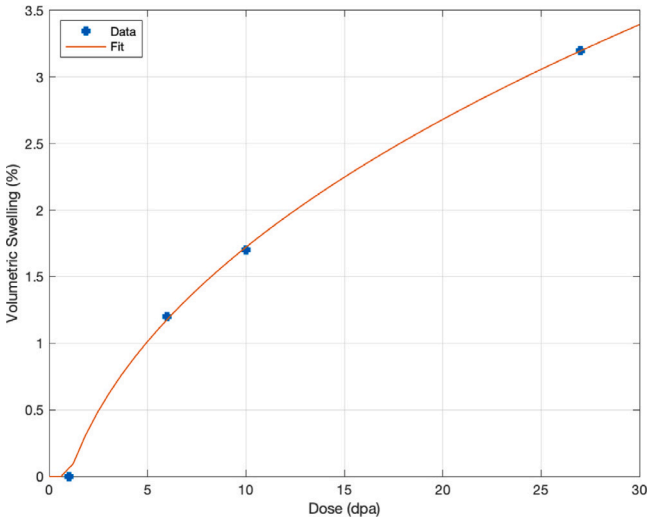

Fig. 7. Swelling rate (%) for different dose rates (dpa). Data from Zhang et al. (2017) is fitted.

The equation used for the fluence factor in the swelling rate ($\text{flux}_{\text{factor}}$) is shown below:

$$\text{flux}_{\text{factor}} = \begin{cases} 0 & \text{dpa} \leq 1.2 \\ a \times \text{dpa}^b + c & \text{dpa} > 1.2 \end{cases} \tag{9}$$

For the temperature factor, a similar correlation to that used for austenitic stainless steel is utilised (using Del Nevo (2014) as reference) because it follows the same *clock* type structure as shown in Fig. 8 from Wright and Sham (2018).

By fitting curves in Fig. 8, the equation from Del Nevo (2014) is modified, as shown in Eq. (10).

$$T_{\text{factor}} = A \exp\left(-\left(\frac{T-490}{100}\right)^2\right) \tag{10}$$

The factor $A = 1.023$ was obtained by calculating the mean over both data sets (17 and 80 dpa) (see Fig. 9).

Swelling is defined as the fractional increase (from $S_{t+\Delta t}$ to S_t) in the volume of the solid with respect to its initial volume (Dickon et al., 2017). The fractional increase is defined in Eq. (11), where the factor 0.01 transforms the value of S_t and $S_{t+\Delta t}$ that are expressed in %. The factor 3 is necessary to transform the volumetric swelling of S_t and $S_{t+\Delta t}$ into a linear strain, assuming isotropic swelling in the three principle directions.

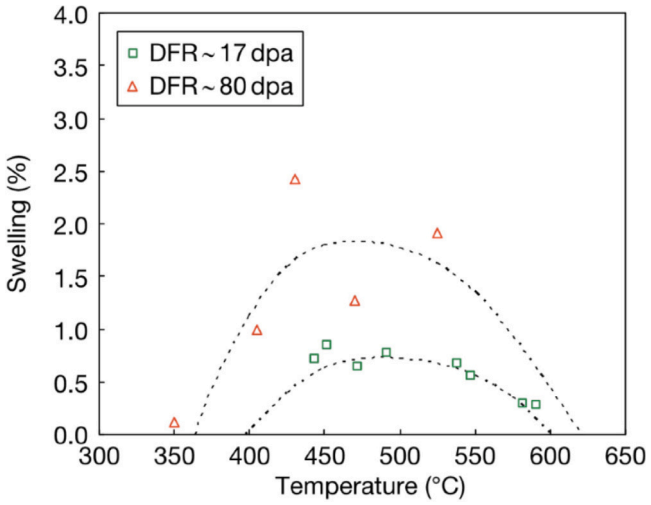

Fig. 8. Swelling rate (%) for different dose rates (dpa) for a range of temperatures. Data from Wright and Sham (2018) DFR (Dual Fluid Reactor).

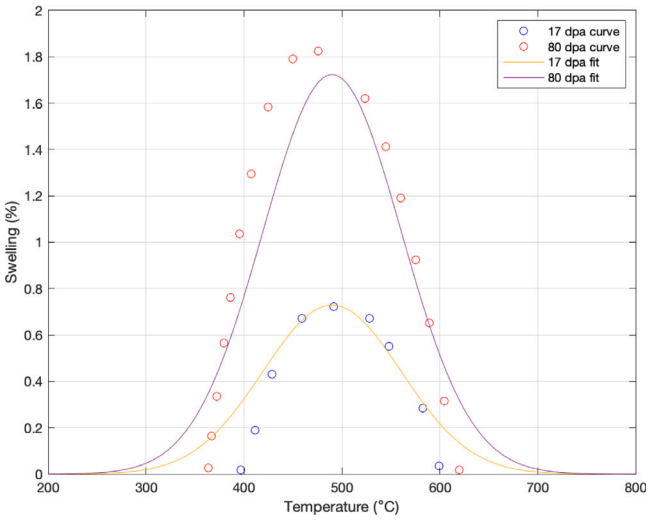

Fig. 9. Fitting curves in Fig. 8 using Eq. (10). By fitting the curves the parameter A = 1.023 in Eq. (10) was obtained. Fit for 17 dpa has an R- Squared of 0.7571, while R-Squared = 0.885 for 80 dpa.

$$\Delta S = \frac{0.01(S_t - S_{t+\Delta t})}{3} \tag{11}$$

For swelling, no other data sources were found in the literature. For this reason, further experiments would be required to verify if the empirical correlation developed matches the behaviour of the alloy.

Creep strain Creep is one of the major concerns when both high temperatures and loads are involved in addition to irradiation effects. TU correlation is focused on the secondary creep as it is the dominating region under normal operation conditions.

Before calculating creep, Larson Miller Parameter (LMP) is determined to ensure that the material does not rupture following the relation implemented in Del Nevo (2014) and using data from Shrestha et al. (2016) for three different temperatures (650 °C, 700 °C and

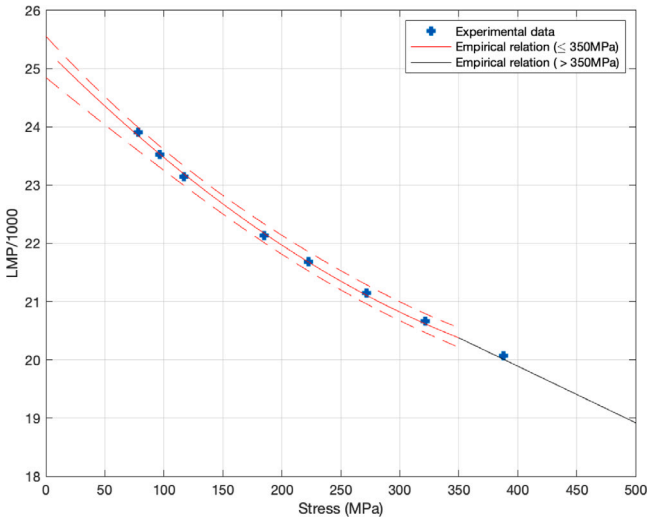

Fig. 10. LMP vs stress (MPa). Data from Shrestha et al. (2016) is fitted. The red dashed line shows the confidence interval (95%) for the first part of Eq. (12).

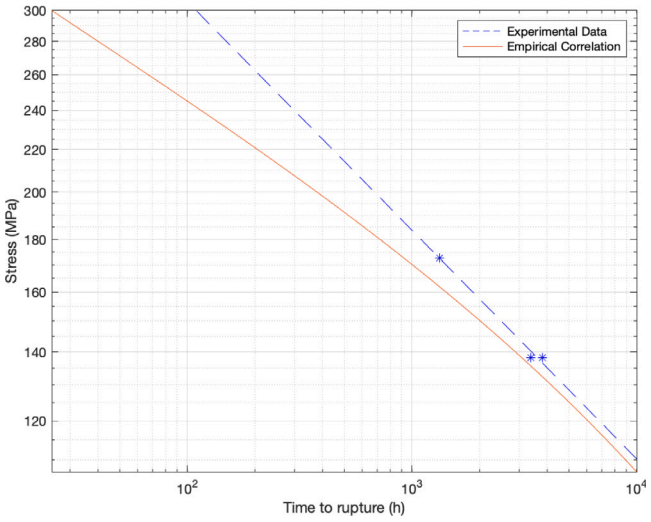

Fig. 11. Time to rupture from Swindeman (1961), the data points and the corresponding fit are from the report. The red line is the empirical relation developed.

750 °C). As displayed in Fig. 10, the available data shows a second order polynomial relation until about $\sigma = 350$ MPa. Then, a linear correlation is implemented to match the values at the higher stress.

$$\text{LMP} = \begin{cases} a_1 \times \sigma^2 + b_1 \times \sigma + c_1 & \sigma \leq 350 \text{ MPa} \\ a_2 \times \sigma + b_2 & \sigma > 350 \text{ MPa} \end{cases} \tag{12}$$

The pressure stress boundary is chosen arbitrarily from the fit as increasing the second order polynomial range would mean an increasing LMP with pressure, which is not physically possible. The followed process is the same as applied by Del Nevo et al. (Del Nevo, 2014) for stainless steel.

The LMP estimates the time to rupture as shown in Eq. (13) with the temperature given in Kelvin.

$$t_{rup} = 10^{\left(\frac{\text{LMP}}{T} - 20\right)} \tag{13}$$

To determine whether the correlation predicts the time of rupture, a set of data from Swindeman (1961) is used. From the ORNL report, only three data points are calculated and fitted using a line in the log–log scale as displayed in Fig. 11. As shown, the correlation is conservative at higher stresses which is desirable when modelling materials for nuclear reactors.

The next step is to calculate the creep of the material. From Venard (1965), the minimum creep rate (h^{-1}) is obtained for three different temperatures. In addition, another set of data from Lee (1967) is used, where verification experiments were performed. In this case, minimum creep rate means creep at the second stage, where it can be considered constant.

The relationship between secondary creep rate and stress can be described using the power law (Zhang, 2010):

$$\dot{\varepsilon}_{\text{II}} = A_T(T)\sigma^n \tag{14}$$

where the constant $A_T(T)$ depends on the temperature and the material, and n is the stress exponent which determines the creep mechanism.

The relationship between secondary creep and temperature is given by an Arrhenius-type equation (Zhang, 2010):

$$\dot{\varepsilon}_{\text{II}} = A_s(\sigma)\exp\left(-\frac{Q_c}{RT}\right) \tag{15}$$

where $A_s(\sigma)$ is a constant that depends on the applied stress, Q_c is the activation energy for creep, R is the ideal gas constant and T is temperature (in Kelvin).

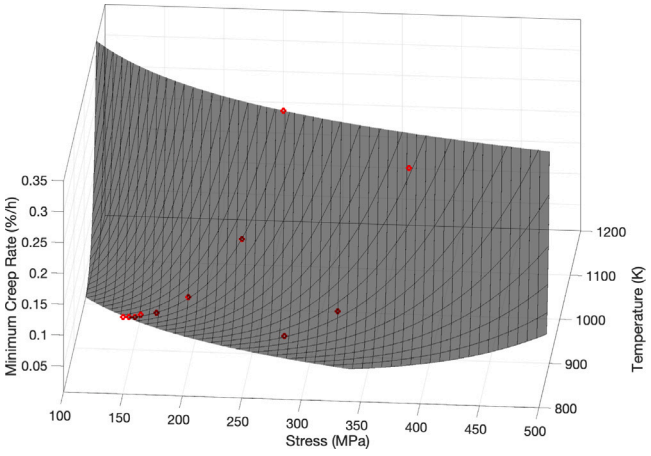

Fig. 12. Creep rate (%/h) against temperature (K) and stress (MPa).

By combining both Eq. (14) and Eq. (15), the final equation for secondary creep is as follows (Zhang, 2010):

$$\dot{\varepsilon}_{\text{II}} = A\sigma^n\exp\left(-\frac{Q_c}{RT}\right) \tag{16}$$

where A is a constant that depends on the material. The coefficients to fit are A and n which are material dependent and Q_c. From Ref. Ji et al. (2015), the average activation energy is estimated to be about 356.3 kJ/mol. This value is greater when compared to that of pure Ni (280 kJ/mol (Thomas et al., 2006)). From Shrestha et al. (2016), the creep mechanism is dislocation creep, the n coefficient taken as 5.9 which lays within the limits of the cited study and its still considered dislocation creep according to Chaturvedi and Han (1989), the exponent of such mechanism is between 3 and 6. The only parameter left to be fitted is A. By using data from Shrestha et al. (2016), $A = 631\ \text{h}^{-1}$. Parameters are summarised in Table A.4. Fig. 12 shows the 3-dimensional fit to obtain the minimum creep rate ($\dot{\varepsilon}_{\text{II}}(\sigma, T)$) where the independent variables are stress and temperature. As expected, the minimum creep rate increases with temperature and stress. Fig. 13 shows a 2-dimensional view of Fig. 13 with the minimum creep rate at three fixed temperatures using stress as the independent variable.

Creep mechanisms depend on temperature and pressure and is affected by irradiation as well. From Zhu et al. (2020), the relationship between dose rate and the change in n coefficient is shown in Fig. 14.

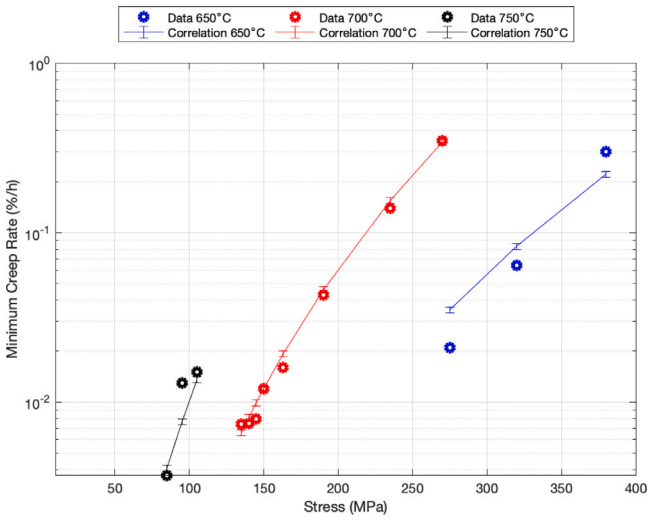

Fig. 13. Creep rate (%/h) against stress (MPa) for different temperatures. The errorbars are calculated by propagation of errors in Eq. (16) with the range of parameters provided in Table A.4.

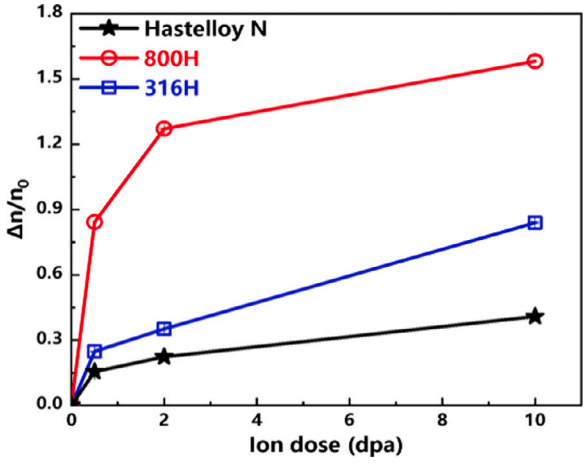

Fig. 14. $\frac{\Delta n}{n_0}$ versus ion dose curves of the Hastelloy N alloy from Zhu et al. (2020). The other alloys in the Figure (800 H and 316 H) are not considered in this study.

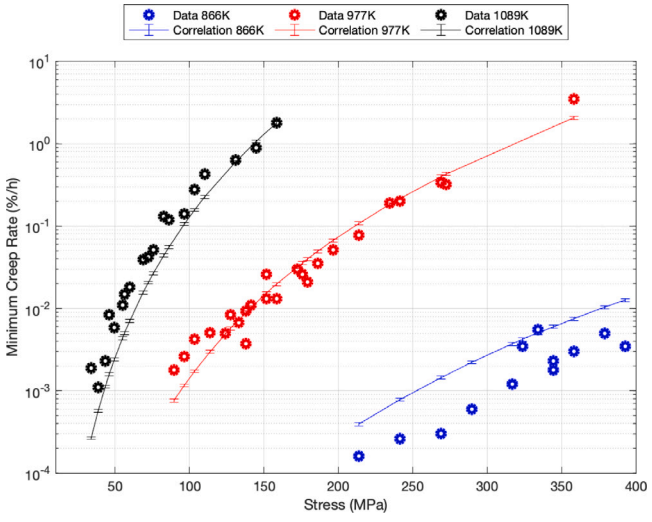

Fig. 15. Creep rate (%/h) against stress (MPa) for different temperatures using data from Swindeman (1961) (unirradiated). The errorbars are calculated by propagation of errors in Eq. (16) with the range of parameters provided in Table A.4. Since the data is unirradiated, either Eqs. (16) or (17) with $n' = n_0$ can be used.

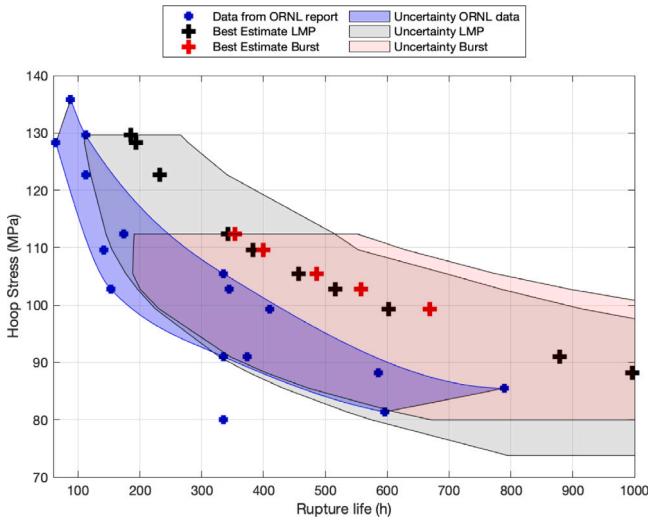

Fig. 16. Results from burst test. In blue, data points from ORNL, the blue shading shows the uncertainty. In red, results from TU burst test using the overpressure criterion, the shading shows the uncertainty. In black, results from TU burst test using the LMP criterion, the shading shows the uncertainty.

Table 3
Uncertainties used in the MC analysis.

Parameter	Uncertainty
Elasticity constant	±15
Yield strength	±15
UTS	±15
Thermal expansion	±15
Thermal conductivity	±15
Outer temperature	±10
Inner radius	−5
Outer pressure	±10
Creep	±20
Swelling	±20

From Fig. 14, coefficient n increases by 0.026 with dose which means that Eq. (16) changes as follows with irradiation:

$$\dot{\varepsilon}_{\mathrm{II}} = A\sigma^{n'} \exp\left(-\frac{Q_c}{RT}\right) \tag{17}$$

$$n' = n_0(a\ \mathrm{dpa}^b + 1) \tag{18}$$

If the irradiation is zero, $n' = n_0$. The conversion from fluence to dpa is the same as for swelling.

For creep strain, correlation (16) was used (since there is no irradiation) with another set of data from a series of tests performed at ORNL (Venard, 1965). Fig. 15 displays the data for several fixed temperatures.

As shown, by calculating the average value of the exponents obtained from data for different temperatures, the correlation agrees better for data at 700 °C and it overestimates for lower temperatures and estimates lower creeps at higher temperatures.

4 First integral assessment

In order to validate the implemented library of material properties, a burst test is performed using the integral TU code. The predicted time to burst is studied according to the LMP and over-stressed criteria and compared to a study conducted by ORNL in the 1960s (Stearns, 1967). The overstress criterion is actually the ultimate tensile stress correlation provided in Eq. (4). A stress-rupture test over three different

Table A.4
Coefficients for the correlations including its value and uncertainty range. The first column is the property, the second column the correlation and the third column the coefficients with the range in brackets. The temperature is in degrees Celsius in all correlations but the creep rate where the temperature is in Kelvin.

Property	Correlation	Coefficients (range)
Elasticity modulus (GPa)	$a\times T^3 + b\times T^2 + c\times T + d$	a = 9.944 $\times 10^{-8}$ (-1.350×10^{-7}, -6.385×10^{-8}) b = 1.178 $\times 10^{-4}$ (6.161×10^{-5}, 1.740×10^{-4}) c = −0.1033 (−0.1277, −0.0789) d = 220.9 (218.3, 223.6)
Yield strength (MPa)	$a \times T^3 + b \times T^2 + c \times T + d$	a = -7.005×10^{-7} (-8.594×10^{-7}, -3.164×10^{-7})) b = 0.001023 (0.000486, 0.001291) c = −0.5319 (−0.6583, −0.3296) d = 334.4 (316.8, 351.8)
UTS (MPa)	$\begin{cases} a_1 \times T'^4 + b_1 \times T'^3 + c_1 \times T'^2 + d_1 \times T' + e_1 & T \le 900\ ^\circ C \\ a_2 + b_2 \times (T - 800) & T > 900\ ^\circ C \end{cases}$	a_1 = 18.60 (5.79, 31.41) b_1 = 2.76 (−10.93, 16.44) c_1 = −121.2 (−161.7, −80.6) d_1 = −190.7 (−219.9, −161.6) e_1 = 635.1 (615.9, 654.3) a_2 = 340.92 b_2 = −1.3
Thermal expansion (μm/m)	$a \times T^2 + b \times T + c$	a = 0.005291 (0.002562, 0.008021) b = 9.682 (6.645, 12.720) c = 107.8 (−637.6, 853.2)
Thermal conductivity (W/m° C)	$a \times T + b$	a = 0.02049 (0.01617, 0.02480) b = 8.431 (6.353, 10.510)
Swelling (%)	$a \times dpa^b + c$	a = 0.9845 (−0.4134, 2.3820) b = 0.4385 (0.1141, 0.7629) c = −0.981 (−2.645, 0.683)
LMP (/)	$\begin{cases} a_1 \times \sigma^2 + b_1 \times \sigma + c_1 & \sigma \le 350\,MPa \\ a_2 \times \sigma + b_2 & \sigma > 350\,MPa \end{cases}$	$a_1 = 1.767 \times 10^{-5}$ (1.276×10^{-5}, 2.258×10^{-5}) b_1 = −0.02033 (−0.02259, −0.01808) c_1 = 25.33 (25.11, 25.55) a_2 = −0.0045 b_2 = 15.4652
Creep rate (%/h)	$A\sigma^{n'} \exp\left(-\frac{Q_c}{RT}\right) n' = n_0(a\ dpa^b + 1)$	A = 631.0 (605.0,657.7) Q_c = 356300 n = 5.9 (5.3, 6.1) a = 0.1774 (0.1482, 0.2065) b = 0.3484 (0.2614, 0.4354) n_0 = 5.9 (5.3, 6.1)

stress levels at a constant temperature of 760 °C was performed. A so-called biaxial specimen was used. It consisted of a hollowed cylinder resembling a cladding. This test was the only biaxial experiment found in the literature as all other tests were performed using uniaxial gauges which cannot be reproduced using TU.

To perform the simulation, the TU in-built Monte Carlo (MC) sampling capability was used to account for uncertainties arising from developing the empirical correlations outlined above and to address the uncertainties surrounding the ORNL experiment as it was mentioned that there was an axial temperature gradient of about ±10 °C. In addition, the dimensions of the specimen were not clearly stated in the report as the sample was coated internally so it is not known if the thickness of the sample already includes the coating or not. This coating was implemented to prevent the sample from oxidation, so it is not useful for the purpose of this study. An uncertainty of 5% was added to the inner radius to account for this issue. An uncertainty in the outer pressure applied was added to account for the possible effect of the coating. Further, since the correlations created are subjected to uncertainties as well, a 15% uniform uncertainty is added to all properties but creep and swelling where a 20% uniform uncertainty is introduced. The uncertainties were derived following a conservative approach from the correlations developed. The Monte Carlo approach in TRANSURANUS code requires on input the upper and lower boundaries expressed in the way shown in Table 3, and the values adopted are also in line with those adopted in the recently published PBNC2022 for FeCrAl (Van Uffelen et al., 2023) and in Ikonen (2016). Creep and swelling are added a greater uncertainty because the Hoop Stress plotted in Fig. 16 was found to be more sensitive to their variations.

A total of 5000 TU MC runs were performed for each of the different stresses and the results were processed using the recently developed TUPython tool which offers an user-friendly GUI that eases the analysis.

As shown in Fig. 16, results obtained using TU overlap with the data from ORNL taking into account the uncertainly of the experiments. Although encouraging for a first integral assessment of the new code version, it also warrants future experimental investigations for a better characterisation of some of the material properties, of which the swelling and creep properties appear to be most important.

5 Conclusions and recommendations

This study summarises the work performed on implementing the material properties of Hastelloy-N, which is an enhanced accident tolerant cladding material of interest for GenIV MSRs, into the TRANSURANUS fuel performance code. Due to the lack of available data, the uncertainties of some of the developed correlations show the necessity of new experiments as most of them were performed in the 1960s and have not been updated. In particular, results from the validation of the thermal conductivity correlation were inconclusive and a separate set of data for the validation of swelling correlation was not found. In addition, creep has been found to have a very important effect at salt-cooled MSR's operating pressures and temperatures. A more exhaustive study is required to determine possible different creep mechanisms at different conditions. Further, the amount of tests under irradiation is not significant which would be required if such material is envisaged for a future pin-type FHR.

In a similar way as for other enhanced accident tolerant materials considered in the frame of the R2CA project, it is therefore recommended to perform additional creep tests at temperatures above 600 °C

to resemble the operating conditions of future salt-cooled MSRs, as well as tests under neutron irradiation in materials research reactors or accelerator facilities to test both irradiation creep and swelling behaviours. Such experiments should be performed using biaxial specimens that match the cladding used in nuclear reactors as it was done in the experiment at ORNL (Stearns, 1967).

A preliminary sensitivity study performed for different stresses showed a strong correlation between the hoop stress and the outer temperature. Moreover, the (absolute) sensitivities to creep and inner radius increase when the stress increases. A complete sensitivity study will be subject to future research.

To conclude, the implementation of Hastelloy-N in TU is still preliminary and subjected to changes should more data become available.

Disclaimer

Views and opinions expressed in this paper reflect only the author's view and the European Commission is not responsible for any use that may be made of the information it contains.

CRediT authorship contribution statement

A. de Lara: Software, Validation, Writing – original draft, Writing – review & editing, Visualization. **A. Schubert:** Software, Validation, Writing – review & editing. **E. Shwageraus:** Writing – review, Funding acquisition, Supervision. **P. Van Uffelen:** Conceptualization, Methodology, Software, Writing – original draft, Writing – review & editing, Funding acquisition, Supervision.

Declaration of competing interest

The authors declare the following financial interests/personal relationships which may be considered as potential competing interests: Paul Van Ufelen reports financial support was provided by European Commission, DG Joint Research Centre.

Data availability

Data will be made available on request.

Acknowledgements

The JRC received funding from the Euratom research and training program 2014–2018 under grant agreement No 847656 for the R2CA project.

Appendix A. Coefficients for the correlations

See Table A.4

References

Anon, 2021. Hastelloy – Density – Strength – Hardness – Melting Point; Available from: https://material-properties.org/hastelloy-density-strength-hardness-melting-point/.

Cen, Q., Tsang, D.K.L., Lu, Y., 2019. Creep damage analysis of thin-walled pressure vessel based on continuum damage model under static loading. Int. J. Press. Vessels Pip. 177, 103994.

Chaturvedi, M., Han, Y., 1989. Creep deformation of Alloy 718. Inst. Aeronaut. Mater.

Del Nevo, A., 2014. Modeling and Analysis of Nuclear Fuel Pin Behavior for Innovative Lead Cooled FBR. ENEA.

Dickon, I., Nuclear Power training Center, Berkeley Nuclear Laboratories, 2017. Transuranus Handbook. Pergamon.

Farkas, M., 1967. Mechanical and Physical Properties of Fuels and Cladding Materials with Potential for Use in Brookhaven's Pulsed Fast Reactor. Battelle Memorial Inst., Columbus, OH (United States).

Field, K.G., Hu, X., Littrell, K.C., Yamamoto, Y., Snead, L.L., 2015. Radiation tolerance of neutron-irradiated model Fe–Cr–Al alloys. J. Nucl. Mater. 465, 746–755.

Gordon, A.J., Walton, K.L., Ghosh, T.K., Loyalka, S.K., Viswanath, D.S., Tompson, R.V., 2012. Hemispherical total emissivity of Hastelloy N with different surface conditions. J. Nucl. Mater. 426 (1–3), 85–95.

Greene, S.R., Gehin, J.C., Holcomb, D.E., Carbajo, J.J., Ilas, D., Cisneros, A.T., et al., 2010. Pre-Conceptual Design of a Fluoride-Salt-Cooled Small Modular Advanced High-Temperature Reactor (SmAHTR). ORNL/TM-2010/199, Oak Ridge National Laboratory.

Guo, P., Xue, J.M., Yan, L., Huang, Q., Li, Z.J., Huai, P., et al., 2015. Irradiation effects in Ni–17Mo–7Cr alloy bombarded with MeV Au ions. Acta Metall. Sin. (English Letters) 28 (7), 903–908.

Guo, S., Zhang, J., Wu, W., Zhou, W., 2018. Corrosion in the molten fluoride and chloride salts and materials development for nuclear applications. Prog. Mater. Sci. 97, 448–487.

Hales, J., Williamson, R., Novascone, S., Pastore, G., Spencer, B., Stafford, D., et al., 2016. BISON Theory Manual the Equations Behind Nuclear Fuel Analysis. Idaho National Lab. (INL), Idaho Falls, ID (United States).

Haubenreich, P.N., Engel, J., 1970. Experience with the molten-salt reactor experiment. Nucl. Appl. Technol. 8 (2), 118–136.

Haynes, T.A., 2018. Finite Element Modelling of Nuclear Fuel Performance in Advanced Gas-Cooled Reactors (Ph.D. thesis). Imperial College London.

Ikonen, T., 2016. Comparison of global sensitivity analysis methods–application to fuel behavior modeling. Nucl. Eng. Des. 297, 72–80.

Jackson, P., Turnbull, J., White, R., 1990. Enigma fuel performance code. Nucl. Energy 29 (2), 107–114.

Ji, Y.q., Qu, S.d., Han, W.x., 2015. Hot deformation and processing map of GH3535 superalloy. Trans. Nonferr. Met. Soc. China 25 (1), 88–94.

Jin, K., Lu, C., Wang, L., Qu, J., Weber, W., Zhang, Y., et al., 2016. Effects of compositional complexity on the ion-irradiation induced swelling and hardening in Ni-containing equiatomic alloys. Scr. Mater. 119, 65–70.

Kamide, H., Rodriguez, G., Guiberteau, P., Kawasaki, N., Hatala, B., Alemberti, A., et al., 2021. Generation IV International Forum-GIF. Annual Report 2020, Organisation for Economic Co-Operation and Development.

Lassmann, K., 1992. TRANSURANUS: a fuel rod analysis code ready for use. J. Nucl. Mater. 188, 295–302.

Lee, S., 1967. Tensile and Stress Rupture Tests of S8DR Hastelloy-N heats: ORNL Verification Tests. Atomics International Div., Canoga Park, CA (USA).

Liu, J., Huang, H., Gao, J., Zhu, Z., Li, Y., 2019. Defects evolution and hardening in the Hastelloy N alloy by subsequent Xe and He ions irradiation. J. Nucl. Mater. 517, 328–336.

Liu, S., Zhang, Y., Wang, X., Tang, M., Zhao, Z., Xu, G., et al., 2015. Investigations on irradiation effects of Ni 60 Nb 40 amorphus alloy and hastelloy-N alloy by 3 MeV Au ion. BEIJING DAXUE XUEBAO (ZIRAN KEXUE BAN) : Beijing Univ. Press 51 (5), 783–790.

Magni, A., Del Nevo, A., Luzzi, L., Rozzia, D., Adorni, M., Schubert, A., et al., 2021. The TRANSURANUS fuel performance code. In: Nuclear Power Plant Design and Analysis Codes. Elsevier, pp. 161–205.

Martin, W., Weir, J., 1965. Effect of elevated-temperature irradiation on Hastelloy N. Nucl. Appl. 1 (2), 160–167.

Oberkampf, W.L., Roy, C.J., 2010. Verification and Validation in Scientific Computing. Cambridge University Press.

Padalko, A., Veselov, A., Avduhin, S., Nipan, G., Sanygin, V., 2003. Differential barothermal analysis (DBA) of Ni-base alloys. J. Therm. Anal. Calorim. 72 (3), 791–799.

Qing-Wan, H., 2010. Curve fitting by curve fitting toolbox of Matlab. Comput. Knowl. Technol. 21, 68.

Scarlat, R.O., Laufer, M.R., Blandford, E.D., Zweibaum, N., Krumwiede, D.L., Cisneros, A.T., et al., 2014. Design and licensing strategies for the fluoride-salt-cooled, high-temperature reactor (FHR) technology. Prog. Nucl. Energy 77, 406–420.

Shrestha, S.L., Bhattacharyya, D., Yuan, G., Li, Z.J., Budzakoska-Testone, E., De Los Reyes, M., et al., 2016. Creep resistance and material degradation of a candidate Ni–Mo–Cr corrosion resistant alloy. Mater. Sci. Eng. A 674, 64–75.

Smith, A., 1965. MSRE Design and Operations Report, Part IX. Safety Procedures and Emergency Plans. Oak Ridge National Lab., Tenn.

Stearns, J., 1967. Determination of Uniaxial Mechanical Properties of Unirradiated and Irradiated Hastelloy-N Bar and Biaxial Stress-Rupture Properties of Chromized and Coated Unirradiated Hastelloy-N. Atomics International Div., Canoga Park, CA (USA).

Swindeman, R., 1961. The Mechanical Properties of INOR-8. Oak Ridge National Lab., Tenn.

Swindeman, R.W., Ren, W., Katcher, M., Holcomb, D.E., 2014a. Hastelloy® N for molten salt reactors used for power generation. In: Pressure Technology, Vol. 40740. American Society of Mechanical Engineers, pp. 288–295.

Swindeman, R.W., Ren, W., Katcher, M., Holcomb, D.E., 2014b. Materials for fossil, nuclear, and petrochemical industries march 25-27, 2014.

Thomas, A., El-Wahabi, M., Cabrera, J., Prado, J., 2006. High temperature deformation of Inconel 718. J. Mater Process. Technol. 177 (1–3), 469–472.

Van Uffelen, P., Hales, J., Li, W., Rossiter, G., Williamson, R., 2018. A review of fuel performance modelling. J. Nucl. Mater. 516 (INL/JOU-18-45934-Rev000).

Van Uffelen, P., Schubert, A., Soti, Z., 2023. Assessing the effect of some ATF materials and uncertainties on their properties under normal operation conditions by means of the transuranus code.

Venard, J., 1965. Tensile and Creep Properties of Inor-8 for the Molten-Salt Reactor Experiment. Oak Ridge National Lab., Tenn.

Watrous, J., 1961. Thermal Expansion of SNAP Materials. Atomics International.

White, J.T., Nelson, A.T., Dunwoody, J.T., Byler, D.D., Safarik, D.J., McClellan, K.J., 2015. Thermophysical properties of U3Si2 to 1773 K. J. Nucl. Mater. 464, 275–280.

Wright, R., Sham, T.-L., 2018. Status of Metallic Structural Materials for Molten Salt Reactors. Idaho National Lab.(INL), Idaho Falls, ID (United States); Argonne National ....

Xing, Z., 2022. Design Space Exploration for Salt Cooled Reactor Systems (Ph.D. thesis). University of Cambridge.

Xu, Z., Jiang, L., Dong, J., Li, Z., Zhou, X., 2015. The effect of silicon on precipitation and decomposition behaviors of M6C carbide in a Ni–Mo–Cr superalloy. J. Alloys Compd. 620, 197–203.

Yadav, A.K., 2016. A review on research trend in corrosion resistant alloy (Hastelloy). Int. J. Inn. Res. Sci. Eng. 2, 310–321.

Zhang, J.S. (Ed.), 2010. 1 - Creep behavior of materials. In: High Temperature Deformation and Fracture of Materials. Woodhead Publishing, ISBN: 978-0-85709-079-9, pp. 3–13. http://dx.doi.org/10.1533/9780857090805.1.3, Available from: https://www.sciencedirect.com/science/article/pii/B978085709079950001X.

Zhang, S., Li, D., Chen, H., Lei, G., Huang, H., Zhang, W., et al., 2017. Ion irradiation-induced swelling and hardening effect of Hastelloy Náalloy. J. Nucl. Mater. 489, 180–186.

Zhu, Z., Huang, H., Liu, J., Ye, L., Zhu, Z., 2020. Nanoindentation study on the creep characteristics and hardness of ion-irradiated alloys. Materials 13 (14), 3132.